Differential Thermography Applied to Structural Integrity Assessment

Jon R. Lesniak, Bradley R. Boyce

Stress Photonics
565 Science Dr. Madison WI, 53711

Abstract

A dual-function for differential-thermographic devices is discussed. It is shown that differential thermographic cameras can be used for rapid inspection of structures as well as for stress analysis. Reviews of Forced Diffusion Thermography (FDT), Thermoelastic Stress Analysis (TSA) and differential thermographic cameras are offered. A new stress intensity measurement technique using TSA data in the vicinity of cracks is described in more detail.

Keywords: Thermography, Thermoelastic Stress Analysis, TSA, Forced Diffusion Thermography, FDT, Cracks

1. Introduction

As the transportation infrastructure continues to age, becoming increasingly suspect, the demand for a new generation of inspection techniques ever increases. Because of the overwhelming vastness of the problems, including aging aircraft and deficient bridges, it is not sufficient to locate cracks and flaws without quantifying their criticality. In the US highway system for example, it is estimated that of the over half a million highway bridges, about 40% are "structurally deficient." The cost of repair or reconstruction could exceed 90 billion dollars. In this era of decreasing budgets, the ability of inspectors not only to isolate cracks but to assess and then prioritize the repair of these structural deficiencies is crucial. This paper demonstrates that Thermoelastic Stress Analysis (TSA) mated to Forced-Diffusion Thermography (FDT) through the shared use of a special differential thermographic camera can meet the demands of the modern NDE era. The same high-speed inspection tool that can seek and isolate cracks can also make a quantitative assessment of the criticality. This paper reviews the ability of FDT to locate cracks in structures and focuses on TSA's ability to quantify the criticality in terms of stress intensity factors.

2. Differential Thermography Technology Primers

2.1 Thermoelastic Stress Analysis Primer

Thermoelastic Stress Analysis (TSA) is a full-field, non-contacting stress-analysis technique. Infrared cameras can be used to measure the small, load-induced temperature changes (ΔT) described by

$$\Delta T = \frac{\alpha T}{\rho C_p}\left(\Delta\sigma_x + \Delta\sigma_y\right) \qquad (1)$$

where ρ is the density, α is the thermal expansion coefficient, Cp is the specific heat, T is the absolute temperature and $\Delta\sigma_x$ and $\Delta\sigma_y$ are the normal stress components. The cameras employed in TSA measure the amplitude of the temperature oscillation, not just the absolute temperature; they are referred to as differential thermographic cameras. To improve measurements, the temperature changes induced by the thermoelastic effect are repeated and time-averaged with continuous dynamic loading. Although sinusoidal loading is most common, more complex load histories like those induced by traffic can be used. Figure 1 is a block diagram of a typical laboratory setup. A closed-loop hydraulic load frame provides the loading while a TSA system correlates the load-induced IR signals with the reference signal from the load cell or strain gage. Most often the differential thermographic camera operates in a lock-in mode, providing in-phase and out-of-phase images. When properly adjusted, the stress map resides in the in-phase image and the out-of-phase image is null.

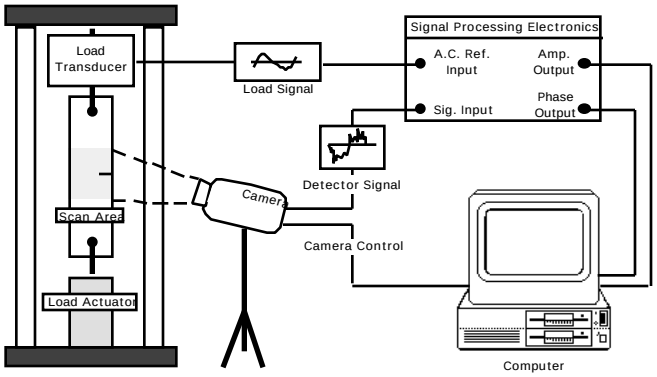

Fig. 1 TSA system block diagram.

2.1 Forced-Diffusion Thermography (FDT) Primer

In general, thermographic NDE techniques have demonstrated the ability to correlate structural integrity with thermal diffusivity[1]. Most often flash lamps are used to uniformly heat the surface of the structure with kilojoule magnitude pulses. However, to find cracks these techniques must rely on the asymmetry of the structure to drive in-plane heat flow across the crack. Several thermographers have found it advantageous to maintain more control over the heat flow. Cramer of Nasa Langley Research Center et al.[2] and Maclachlan Spicer et al.[3] have both used line flux sources. These techniques inspect a linear region for cracks parallel and adjacent to the hot line. Wang of Wayne State University developed a point heating technique referred to as the "flying spot" technique. The flying spot technique scans the object to create a full field image.

FDT extends the concept of spatially varied heat flux to full-field[4]. Instead of a point or single line of flux, it projects a continuously-emitted, full-field, dynamic heat pattern onto the surface of the structure (Fig. 2). The resulting thermal distribution is dynamic which allows the use of the more sensitive differential thermographic cameras. The use of continuos radiation reduces the wattage of the source to a safe level, about 500 watts. Flaws such as cracks or delaminations impede the flow of heat resulting in distinct temperature signatures. The spatial and temporal frequencies of the dynamic heat pattern can be adjusted to control the levels of lateral and through-depth heat flow to target general or specific flaws.

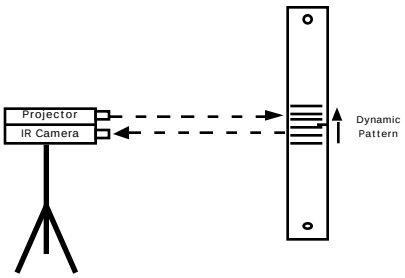

Fig. 2 Forced-diffusion thermography.

The most basic and perhaps useful pattern is the moving line pattern. Not only does the heat sink into the structure but it flows from hot stripe to "cool" stripe. The moving line pattern is mathematically described as

$$q(x,t) = \frac{C}{2}\left[1+\cos(2\eta\pi x + \omega t)\right] \qquad (2)$$

where C is the light intensity, η is the line density and ω is the temporal frequency. The flux at a particular value of x is a continuos oscillation at frequency ω with phase shift $2\eta\pi x$. The flux gradient with respect to x is

$$\frac{\partial}{\partial x} q(x,t) = \eta\pi C\cos(2\eta\pi x + \omega t) \qquad (3)$$

The flux gradient oscillates as well which serves to drive heat back and forth across the crack. Of course, the exact phase of the heat flow is determined by the heat transfer and the resulting thermal distribution. At a given temporal frequency, decreased line densities decrease the heat flow from "hot" to "cool" stripes and therefore increase flow into the structure. It is important to note that all points over the field-of-view of the camera are simultaneously driven with the same flux gradient that optimizes speed and the probability of locating flaws.

The differential thermographic camera views the moving line pattern as an in-phase and out-of-phase image, but for FDT this does not have meaning. Unlike TSA, all points in the FDT field have a different phase. For the purpose of this discussion, it is assumed that the phase of the system is adjusted so that in-phase refers to a temporal cosine and out-of-phase refers to a temporal sine. Rewriting Eq. 2 as

$$q(x,t) = \frac{C}{2}\left[1+\cos(2\eta\pi x)\cos(\omega t) + \sin(2\eta\pi x)\sin(\omega t)\right] \qquad (4)$$

it is apparent that the moving line pattern can be thought of as a superposition of an in-phase spatial cosine and an out-of-phase spatial sine pattern. Figure 3 shows the results of a numerical model of the effect this heating pattern has along a line across a crack. It clearly shows the effects of the discontinuities on the sine, cosine and amplitude image.

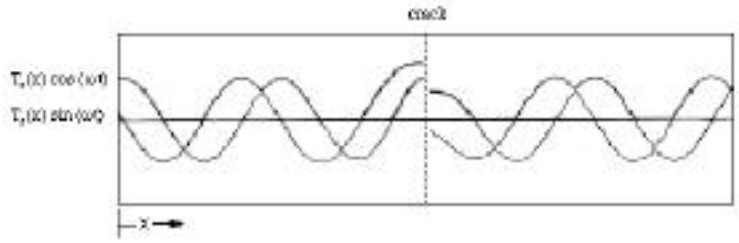

(a) temporal components

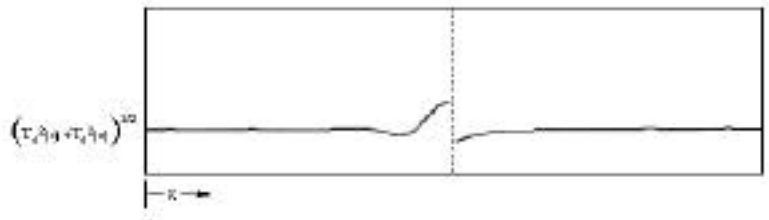

(b) amplitude

Fig. 3 Numerical model of FDT applied to cracked plate.

It is often difficult to process the striped in-phase and out-of-phase images for cracks. Instead, crack identification can be accomplished by applying an edge filter to the amplitude image as seen in Fig. 4. This is an example of a fatigue crack in 1/16 thick aluminum. More sophisticated uses of the data are under development.

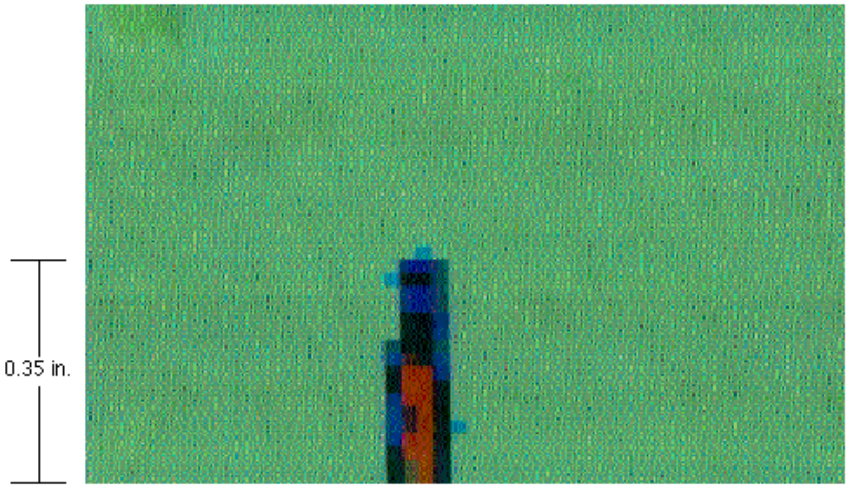

Fig. 4 FDT amplitude image filtered for cracks.

3. Differential Thermographic Camera

This report embodies results using two different TSA systems: a SPATE 9000 and a DeltaTherm 1000. The DeltaTherm 1000 is based on an 128 x 128 InSb focal plane array (FPA), the development of which was performed by the authors under a NASA-Langley funded Phase II SBIR. This camera uses digital processing described by

$$B = \frac{2}{N}\sum_{n=1}^{N} y_n \sin\beta(n) \qquad (5)$$

where B is the amplitude of the signal, y_n is the sampled signal, N is the number of samples, and $\sin\beta(n)$ is a reference provided by a load or strain transducer in the case of TSA and is provided by the projector in the case of FDT. Currently only periodic references are usable, but circuit designs allowing random loads are nearly ready for implementation. In either mode of operation the signal-to-noise ratio improves with the inverse root of time. Some of the data shown in this paper was collected in the earlier stages of development of the array camera; therefore, the data does not benefit from the use of non-uniformity correction maps. A non-uniformity correction map calibrates the variance in the sensitivities of the multitude of detectors present in the array. Fortunately, this does not seem to be critical to stress intensity measurements as will be described. Figure 5 represents an earlier state of the array camera's abilities; this digitally sampled stress image of a crack in aluminum was collected in 10 seconds.

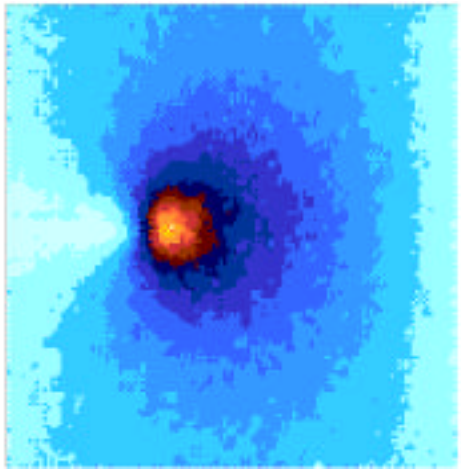

Fig. 5 Example TSA image from array camera.

The SPATE 9000 uses a single detector that is step-scanned across the object to create a full field image. It spends about 0.2 seconds at each point utilizing an analog lock-in amplifier to correlate the load or heat source frequency to the thermal signal. The authors have developed digital signal processing for the step scan system that allows correlation of random reference signals, which is often necessary in order to quantify stresses from live loading.

4. Quantitative Fracture Mechanics, Least Squares Method

The development of quantitative fracture mechanics was funded by Wright-Patterson AFB through a phase I SBIR grant[5]. The goal of this portion of the project was to develop a reliable and quantitative method of making stress intensity measurements from the data provided by a differential thermographic camera. This ability coupled with developments in random load input will allow for efficient quantification of the criticality of cracks in live structures. Previous efforts were reviewed [6],[7],[8] and although the efforts represent a great contribution to the task at hand, they were found not to offer the potential in applicability and accuracy that are required to make reliable stress intensity measurements via TSA. Improvements on these works developed as a result of this project include accommodation of more terms in stress functions and the full utilization of the available data field. Also, thermal conduction and optical limitations are considered.

4.1 Increased Terms in Stress Function

William developed theories stating that there are a set of fundamental stress features that can exist in the region around a crack in a plate[9]. He sought Airy's stress functions under the coordinate system described in Fig. 6. By taking the appropriate derivatives and combining the normal stresses to get the sum of the principal stresses, the fundamental stress features for a Mode I cracked plate can be found. The first four terms of which are

$$A_{-1/2} = \frac{2}{\sqrt{2\pi r}}\cos(\theta/2) \qquad \lambda_I = -1/2 \qquad (6a)$$

$$A_0 = 1 \qquad \lambda_I = 0 \qquad (6b)$$

$$A_{1/2} = r^{\frac{1}{2}}\cos(\theta/2) \qquad \lambda_I = 1/2 \qquad (6c)$$

$$A_1 = r\cos(\theta) \qquad \lambda_I = 1 \qquad (6d)$$

The first term resembles a cardioid shape seen in Fig. 5 and detailed in Fig. 6.

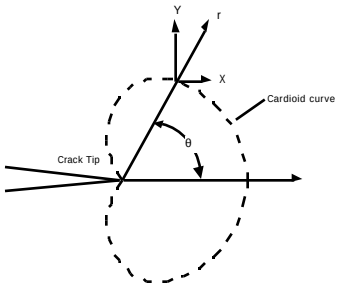

Fig. 6 Stress-function coordinate system.

Although the cardioid shape is generally predominant, the total stress field can be written as a combination of the basic stress shapes

$$\{S\}_n = \left[\{A_{-1/2}\}_n \quad \{A_0\}_n \quad \{A_{1/2}\}_n \quad \{A_1\}_n\right] \begin{Bmatrix} C_{-1/2} \\ C_0 \\ C_{1/2} \\ C_1 \end{Bmatrix} \tag{7}$$

As can be seen, only the λ=-1/2 term of Eq. 6a is of significance at the crack tip where it is singular. It is this stress feature that causes crack growth and for this reason, classical fracture mechanics ignores the remaining terms and defines the stress intensity factors from the $\lambda = -1/2$ terms as

$$K_I = C_{\lambda_I = -1/2} \tag{8}$$

Although the stress intensity factors are determined solely by the $\lambda = -1/2$ terms, it is important to account for all terms in the analysis. As a practical matter, the data around the crack tip cannot be used because of

- Inelastic material behavior
- Heat conduction
- Optical limitations

This means that the analysis must utilize data from the stress field that is not necessarily dominated by the $\lambda = -1/2$ terms. Figure 7 compares the stress distribution of the λ=-1/2 term with that of the λ =1 term for θ =0. It can be seen that data far from the tip can be influenced greatly by the other terms.

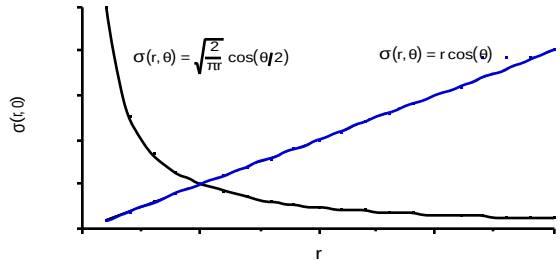

Fig. 7 Influence of higher-order terms on crack tip stresses.

4.2 Stress Intensity Measurement via Least Squares Fitting

To avoid the potential inaccuracies, a new method of determining stress intensity factors from thermoelastic data was derived. It involves least square fitting all pertinent terms to the data so that a better estimation of the magnitude of the stress intensity factor can be obtained. Equation 7 can be written more simply as

$$\{S\} = [Q]\{C\} \tag{9}$$

where [Q] is the vector of stress features. The least squares algorithm applied to Eq. 9 yields

$$[Q]^T\{S\} = [Q]^T[Q]\{C\} \tag{10}$$

To simplify the least square algorithm, the basis is orthogonalized and normalized over the fit window so that

$$[Q']^T\{S\} = \{C'\} \tag{11}$$

This allows for rapid application and re-application of the fit. The values of {C}, and therefore the stress intensity factor, can be determined from {C'}.

4.3 Mixed Mode Stress Intensity Measurement

The same algorithm as defined by Eq. 11 can be derived for mixed-mode cases by the addition of the Mode II stress shape terms in Eq. 7. The total stress state for mixed Mode I and Mode II is described by

$$\{S\}_n = \left[\{A_{-1/2}\}_n \quad \{A_0\}_n \quad \{A_{1/2}\}_n \quad \{B_{-1/2}\}_n \quad \{B_0\}_n \quad \{B_{1/2}\}_n\right] \begin{Bmatrix} C_{I,-1/2} \\ C_{I,0} \\ C_{I,1/2} \\ C_{II,-1/2} \\ C_{II,0} \\ C_{II,1/2} \end{Bmatrix} \tag{12}$$

where A represents the features of Mode I and B represents the features of Mode II. Only the first three terms are used for brevity. The Mode I stress intensity factor is based on the $A_{-1/2}$ stress shape and is derived from $C_{\lambda I=-1/2}$, and the Mode II stress intensity factor is based on $B_{-1/2}$ stress shape and is derived from $C_{\lambda II=-1/2}$.

5.0 Stress Intensity Measurement Test Results

At the onset of this project the array camera was not available, so the SPATE 9000 camera was used in the stress intensity quantification study. Simple pin-connected 1018 steel specimens were used in the stress intensity verification study (Fig. 8). Three specimen geometries were used with EDM notches of a/w ratios of 0.097, 0.30, 0.50. The specimens having thickness of 1.6 mm are considered to be in a plane-stress state.

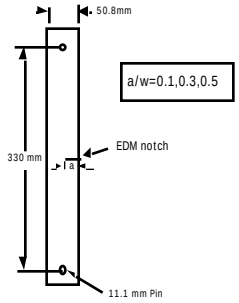

Fig. 8 Fracture mechanics specimen configuration.

Figure 9 shows the full-view TSA images for the three crack lengths. Close-up scans are used for the stress intensity measurement.

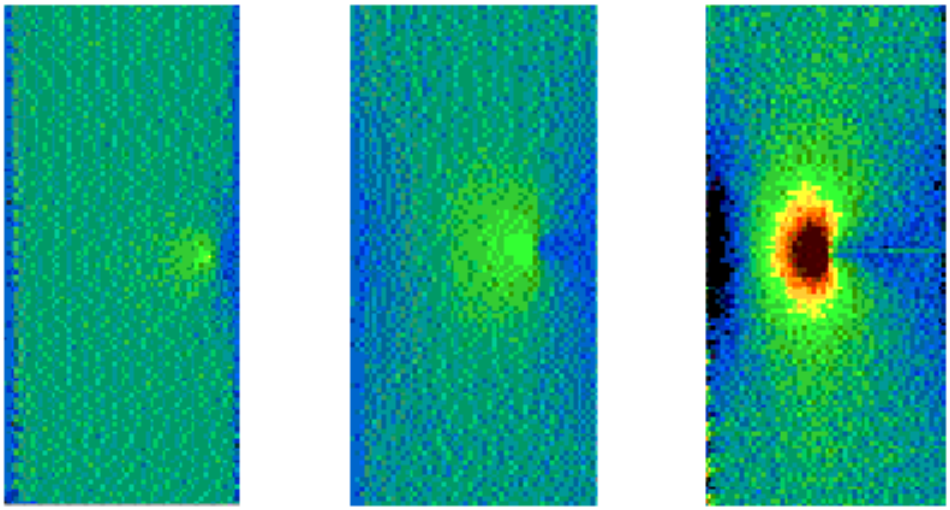

(a) a/w=0.097 (b) a/w=0.30 (c) a/w=0.50

Fig. 9 Full-view TSA images of fracture specimens.

The data around the crack tip is not used in the fit for reasons previously described. The data used in the least squares fit includes the data lying within the box, excluding the data in the circle (Fig. 10). The fit area is about 10mm square. Figure 10a shows the in-phase close-up stress image and 10b shows the out-of-phase stress image for a/w= 0.1. In-phase refers to the fact that the

oscillating thermal signal is synchronized with the applied oscillating load. Out-of-phase signal occurs when inelastic events or heat transfer are present. From the out-of-phase image, the minimum acceptable radius of the fit window can be determined.

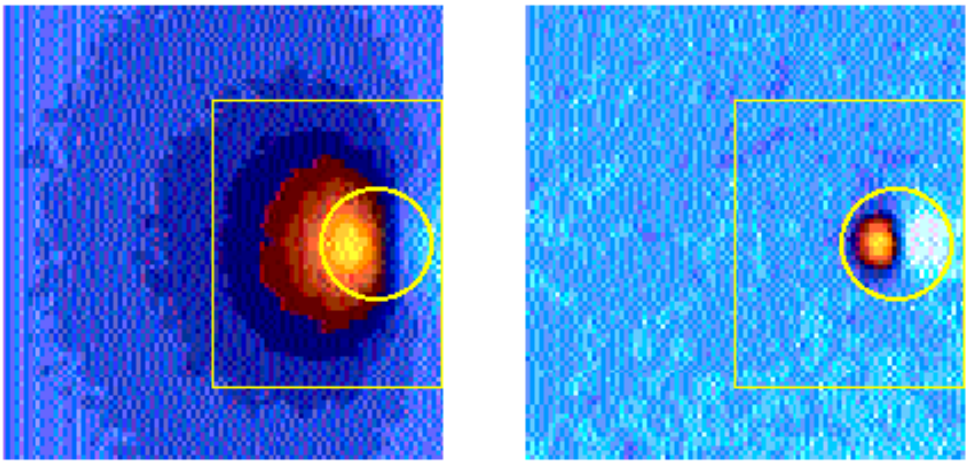

(a) in-phase TSA image (b) out-of-phase TSA image

Fig. 10 In-phase and out-of-phase TSA images.

Erroneous stress intensity measurements resulting from either insufficient stress terms or incorrect assumptions of tip location are clearly identified through an error estimator. By reiterating the fit over a small area of potential tip positions and optimizing the error estimator, the tip location can be found within one camera pixel.

TSA directly measures the stress intensity factor. It does require knowledge of the thermoelastic response of the material (i.e., the thermal properties in Eq. 1), but these can be easily determined for each material from a simple uniaxial bar experiment, the results of which are valid for all applications of that material. Figure 11 shows the ability of TSA to quantify stress intensity factors. The quantified values of Y as defined in Fig. 11 for the three geometries are plotted vs. a/w for the four-term and one-term fit estimations and the theoretical solution[11].

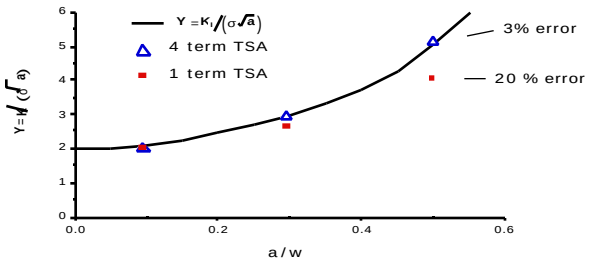

Fig. 11 Y vs. a/w, 1-term and 4-term fit compared to theoretical data.

The 4-term fit and a more appropriate use of crack tip data affords significant improvement in stress intensity measurements. Simulations indicate an equal accuracy in determining mixed-mode stress intensity factors.

6. Conclusions

It is apparent that TSA will provide a powerful tool in the assessment of flaw criticality. More development is needed to extend the assessment ability to a wider range of crack types. Still, because a healthy traffic flow is necessary to acquire data, TSA may not be an efficient high-speed inspection technique in all situations. Instead, FDT is a self-sufficient technique that can seek and locate flaws. The following scenario might become common place. First, a bridge undergoes its routine inspection with the benefit of FDT. As a result, the cracks are isolated and can be assessed using the TSA fracture mechanics approach. Also, a more general stress analysis can be provided by TSA. Next, a scale simulation of the bridge detail can be set up in the lab taking care to ensure that the TSA information from the bridge site matches the TSA information in the simulation. The bridge design team can then design and redesign retrofits in an efficient and less costly environment. Once the retrofit is designed, a field test can be performed and the stresses can again be assessed using TSA. Once it is confirmed that the retrofit modifies the stress as designed and it is shown that the stresses are not chased to another part of the structure, the retrofit can be replicated over the plethora of similar bridge details.

References

1. L.D. Favro, D.J. Crowther, P.K. Kuo and R.L. Thomas, "Inversion of pulsed thermal-wave images for defect sizing and shape recovery, "Thermosense XIV, Jan K. Eklund, Editor, Proc. SPIE 1682,178-181,1992.

2. K.E. Cramer and W.P.WInfree,"Thermographic Imaging of Cracks in Thin Metal Sheets", Thermosense XIV, Jan. K. Eklund, Editor, Proc. SPIE 1682,162-170,1992.

3. J.W. Maclchlan Spicer, W.D. Kerns,L.C. Aamodt and J.C. Murphy, "Source patterning in time-resolved infrared radiometry (TRIR) of composite structures," Thermosense XIV, Jan K.Eklund Editor, PRoc. SIE 1682,248-257,1992.

4. Lesniak, J.R. and Boyce, B.R., "Forced-Diffusion Thermography," Proc. SPIE Nondestructive Inspection of Aging Aircraft, San Diego, July 1993, Vol. 2001, pp. 92-102.

5. Lesniak, J.R., "Differential Thermography for Extreme-Environment Structural Integrity Measurements, "Phase I SBIR Final Report,1994

6. Stanely, P. and Chan, W.K., "The determination of Stress intensity factors and crack-tip velocities from thermoelastic infra-red emissions," Proc. Int. Conf. on fatigue of Engineering Materials and Structures , Sheffield,1986,Vol. 1,pp. 105-114.

7. Stanely, P. and Chan, W.K., "Mode II crack studies using SPATE Technique," Proc. SEM Spring Conf. on Experimental Mechanics, New Orleans, 1986, pp. 916-923.

8. Stanely, P. and Dulieu-Smith, J.M., "Progress in the Thermoelastic Evaluation of Mixed Mode Stress-Intensity Factors," Proc. SEM Spring Conf. on Experimental Mechanics, Dearborn, June 1993, pp. 617-623.

9. Williams, M.L., "On the Stress Distribution at the Base of a Stationary Crack," J. Appl. Mech.,Vol. 24, pp. 109-114, 1957.